Desalination 404 (2017) 59–71

Contents lists available at ScienceDirect

Desalination

journal homepage: www.elsevier.com/locate/desal

Development of an integrated hybrid solar thermal power system with thermoelectric generator for desalination and power production

Murat Emre Demir [a,*], Ibrahim Dincer [a,b]

[a] Clean Energy Research Laboratory, Faculty of Engineering and Applied Science, University of Ontario Institute of Technology, 2000 Simcoe Street North, Oshawa, Ontario L1H 7K4, Canada
[b] Faculty of Mechanical Engineering, Yildiz Technical University, Besiktas, Istanbul, Turkey

HIGHLIGHTS

- An integrated desalination system is developed.
- A thermoelectric unit is incorporated into the integrated system.
- An efficiency assessment of the integrated system is performed through energy and exergy efficiencies.
- A parametric study is undertaken to investigate how operating conditions affect the system performance.

ARTICLE INFO

Article history:
Received 2 May 2016
Received in revised form 28 October 2016
Accepted 28 October 2016
Available online 5 November 2016

Keywords:
Desalination
Power generation
Thermoelectric generator
Volumetric solar receiver
Solar gas turbine
Exergy efficiency
Flash distillation

ABSTRACT

In this study, an integrated system for desalinated water and electricity production is developed and thermodynamically analyzed. The proposed system consists of a solar-natural gas hybrid power plant, thermoelectric generator (TEG), Rankine cycle to produce electricity and flash distillation unit to produce fresh water. The proposed electricity-fresh water co-generation plant uses solar driven volumetric pressurized air receivers as main power supply and uses natural gas to compensate power when the direct normal irradiance is below 900 W/m^2. Thermoelectric materials are used to generate electricity from waste heat of gas turbine. Flash distillation unit is used to produce fresh water from seawater by the waste heat of Rankine cycle. All thermodynamic quantities, such as energy and exergy efficiencies, exergy destructions are calculated for all system components. The combustion reaction is modelled on ASPEN Plus software package. TEG unit is modelled on COMSOL Multiphysics software package, and the rest of the elements of the system are analyzed in the Engineering Equation Solver (EES). The overall exergy and energy efficiencies of the system are determined to be 54.9% and 44.5% respectively where the total energy input comes 50% from solar system and 50% from natural gas. The results show that TEG unit can generate power more than 32 kW by using the waste heat. The present results indicate that it is possible to produce 3.36 kg/s of fresh water from proposed system. Furthermore, the effects of direct normal irradiance level, ambient wind speed, seawater temperature, various cool side cooling options for the thermoelectric generator on the system performance are investigated.

1. Introduction

The purpose of using renewable energies is mainly reducing carbon emissions in the world. CO_2 emissions are expected to cause a very vital problem in the world as the growth rate of the population and quality of life continue rising [1]. The most significant benefit of solar energy, when it is compared with other energy sources, is that it is clean and can be provided without any ecological pollution. Fossil fuels have supplied most of the world's energy demand over the past century. As they are less inexpensive and more useful than energy from alternative energy sources, they are more preferable. By the development of solar power systems, it is possible to operate a gas turbine with direct normal heating of pressurized air.

In 2005, the European Commission [1] published their final report on SOLGATE project. In their project, a volumetric solar receiver is developed to heat up the pressurized air to 1000 °C. Hot pressurized air provides energy to gas turbine. Peng et al. [2] proposed a solar tower thermal power system integrating the intercooled gas turbine top cycle and the Kalina bottoming cycle. Solar part of the proposed system is using pressurized air receivers as in SOLGATE project. Consequently, the highest solar-to-electric efficiency of the suggested system is obtained 27.5% at a gas turbine inlet temperature of 1000 °C.

* Corresponding author.
E-mail addresses: murat.demir@uoit.ca (M.E. Demir), ibrahim.dincer@uoit.ca (I. Dincer).

http://dx.doi.org/10.1016/j.desal.2016.10.016
0011-9164/

Nomenclature

Cp	Specific heat at constant pressure (kJ/K)
DNI	Direct normal irradiance (W/m^2)
$\dot{E}x$	Exergy rate (kW)
ex	Specific exergy (kJ/kg)
h	Specific enthalpy (kJ/kg)
k	Thermal conductivity (W/m K)
LHV	Lower heating value (kJ/kg)
$\dot{m}$	Mass flow rate (kg/s)
P	Pressure (kPa)
$\dot{Q}$	Heat rate (kW)
s	Specific entropy (kJ/kg K)
S	Seebeck Coefficient (V/K)
T	Temperature (K)
X	Salinity (ppm)
$\dot{W}$	Work rate (kW)

Greek letters

η_{en}	Energy efficiency
η_{ex}	Exergy efficiency
σ	Electrical conductivity (S/m)
σ_{SB}	Stefan Boltzmann constant (5.76 10^{-8} W/m^2 K^4)
E	Surface emissivity

Subscripts and superscripts

b	Brine water
cw	Cooling seawater
C	Compressor
CC	Combustion chamber
Ch	Chemical
d	Destruction
de	Desalinated water
f	Intake seawater
field	Heliostat field
GT	Gas turbine
HEX	Heat Exchanger
i	State number
In	Inlet of a component
n	n-type thermoelectric material
NG	Natural Gas
Out	Outlet of a component
ov	Overall
P	Pump
p	p-Type thermoelectric material
Ph	Physical
Sys	System
ST	Steam turbine
T	Turbine
ZT	Dimensionless figure of merit
0	Ambient condition
1, 2, … i	State points

Acronyms

C	Compressor
CO_2	Carbon dioxide
EES	Engineering Equation Solver
FDU	Flash Distillation Unit
HEX	Heat exchanger
N	Total number
PR	Performance Ratio
TEG	Thermoelectric generator

Meriche et al. [3] proposed a hybrid solar tower power plant using pressurized air receiver and investigate it with and without the presence of regenerator. The suggested power plant has 27% and 33% overall thermal efficiency with and without the presence of regenerator, respectively.

Thermoelectric materials are semiconductor materials, which can convert heat to electricity by Seebeck effect and vice versa. As thermoelectric generators do not have any moving parts, they are easy to operate and have low maintenance cost. Hence utilization of these systems is a reasonable method to generate clean energy. However, thermoelectric generators have low thermal efficiencies [4]. As a result of this situation, they are mostly used for waste heat management applications. Orr et al. [5] made an experimental work for waste heat recovery from exhaust gases of a car by using thermoelectric cells. The temperature difference between hot and cold sides of the thermoelectric cells was maintained by heat pipes in the proposed system. As a result of their study, the maximum power which the cells can produce was 6.03 W with 1.43% efficiency. Omer and Infield [6] proposed a two-stage parabolic concentrator and thermoelectric materials be attached on absorber plates to use waste heat. Sahin et al. [7] also made a similar study by investigating the performance of a conventional solar concentration power plant with and without the presence of thermoelectric devices. In the suggested system, thermoelectric devices are installed on heat collector element. As a result, the thermal efficiency of the system with thermoelectric devices is calculated slightly higher than the same system without the thermoelectric generators. Thermoelectric generators are also used to recover the waste heat of gas turbines. Francis et al. [8] proposed a gas turbine system in which the efficiency was increased by 10% with the presence of thermoelectric generator.

Desalination is a technology to get rid of dissolved solids and ions from briny water, seawater, or industrial wastewater. The purpose is to produce clean water from seawater or brackish water or recover polluted water in an engineering process [9]. Desalination technologies can be categorized as the membrane-based and thermal-based separation processes. Reverse osmosis (RO), multi-stage flash (MSF), and multi-effect distillation (MED) are the core technologies for commercial-scale [9]. Khalid et al. [10] made a comparative assessment of two systems for nuclear desalination. The systems use Reverse Osmosis (RO) for desalination and are coupled with either a CANDU 6 nuclear reactor or a Sodium-cooled Fast Reactor (SFR). As a result of the study, the cogeneration exergy efficiency and RO process exergy efficiency of the CANDU 6-based system are obtained higher than the SFR-based system. Cardona et al. [11] proposed an integrated system for the desalination of the seawater. In the proposed system, reverse osmosis and multistage flash distillation units connected in series. As a result of the study, the proposed plant provides cost reduction for the fresh water, when it is compared to the equivalent systems in parallel. Hawlader et al. [12] proposed and built a system with a single effect desalination unit. The desalination unit is connected to a solar assisted heat pump. They investigated the effects of feed seawater temperature and flashing. As a result, the maximum performance ratio of the desalination unit is obtained 1.15.

Seawater desalination plants with solar thermal power are considered a clean way to produce fresh water from seawater. There are various applications in this area such as solar energy multi-stage flash systems (MSF), solar energy MED systems, solar energy compressing distillation systems, etc. For example, a solar energy driven multi-stage flash desalination system was constructed in Kuwait with a 7000-liter reservoir and a 220 m groove-shaped parabolic heat collector and a capacity of 10 t of fresh water per day [13]. Ortega-Delgado [14] made a thermo-economic analysis of electricity and water cogenerative Solar Thermal Power Plant (STPP) of 5 MW. Their system is equipped with parabolic trough mirrors and Direct Steam Generation (DSG). They compared two distillation technologies which were Multi-Effect Distillation (MED) and Reverse Osmosis (RO) to find the best arrangement of integration with the STPP. An average daily operation of the

system (with fresh water production, plant capacity, net electric and thermal power consumption, specific consumption of auxiliaries and specific consumption of the process) is taken into account to choose the best option. Their results show that the best integrated system choice is with the reverse osmosis unit which is connected to the local electric grid [14]. Palenzuela et al. [15] proposed four different combined concentrating solar power plants with a large-scale desalination plant. In their system, it is possible to produce fresh water from reverse osmosis and thermal desalination systems. As they coupled reverse osmosis and thermal desalination plants with CSP plant, they reduced the cooling load on CSP and recovered the waste heat of it while producing fresh water. It is possible to produce 47,723 m^3/kg fresh water per day and 62.42 MWe energy. Palenzuela et al. [16] made another study of performance assessment of different potential desalination units integrated with concentrating solar power plant. They investigated low-temperature multi-effect distillation and thermal vapor compression multi-effect distillation combined with a concentrating solar power plant. They also connected a reverse osmosis unit to the plant as an alternative configuration. Palenzuela et al. [17] investigated four different configurations of the CSP based desalination system in arid regions. Their system was capable of generating 50 MWe power and producing 48,498 m^3/day fresh water. In regards to the plants with smaller capacities, there are various studies focused on relatively small-scale concentrated solar based desalination systems [18–20]. Iaquniello et al. [18] proposed a system which consists of a CSP plant integrated with MED-RO distillation unit to be able to produce around 20,000 m^3 fresh water per day.

Garcia-Rodriguez et al. [21] investigated solar assisted multi-stage flash distillation systems. They made a comprehensive comparison between a traditional MSF system with a solar assisted one. For the solar assisted MSF system solar collectors heat the brine when the sunlight is available, and during night, a traditional energy supply runs the MSF system. The climatic conditions, desalination plant capacity and performance ratio of the system, and costs are taken into account in the study. As a result, the study indicates that solar-assisted systems can be profitable compared to conventional MSF systems. Furthermore, potential price reduction on parabolic through collectors and cost rising in the fossil fuels will affect the competitiveness of solar energy in MSF plants notably.

In this study, a water-electric cogeneration system is developed. The proposed system consists of the solar-natural gas hybrid power plant, thermoelectric generator (TEG), Rankine cycle and Flash distillation unit for producing fresh water. The combined co-generation power-desalination plant uses volumetric pressurized solar receivers as main power supply and uses natural gas to compensate the deficient power when the direct normal irradiance is below 900 W/m^2.

Thermoelectric materials are used to generate electricity from waste heat of gas turbine and flash distillation unit is used to produce fresh water from seawater from waste heat of Rankine cycle. Both components utilize the waste heat and increase the overall efficiency of the system. Both TEG and FDU are also selected as environmentally friendly components. Neither of them causes any greenhouse gas emissions while producing their products which affects the environmental impact of the system positively. They both are simple designs. TEG has no moving part, what makes its maintenance cost cheap. FDU has only pumps as moving parts. By using solar power, thermoelectric effect and flash distillation it is aimed to produce clean energy and water.

All thermodynamic parameters, such as energy and exergy efficiencies, exergy destructions, temperature, pressure, specific enthalpy and entropy are calculated for all system components. The combustion reaction is modelled on ASPEN Plus software package. TEG unit is modelled on COMSOL Multiphysics software package and rest of the components of the system is constructed in the Engineering Equation Solver (EES). Furthermore, the effects of solar radiation level, ambient wind speed, seawater temperature, thermoelectric generator cool side cooling method are investigated.

2. System description

In this study, a water-electric cogeneration hybrid system is designed to meet a small seaside town's electricity and fresh water demands. Thermoelectric materials are used to generate electricity from waste heat and enhance overall system efficiency. The system is designed as the schematic is presented in Fig. 1.

In the suggested system, main outputs from the system are distilled water and electricity, while main inputs are air, water and seawater. The system consists of a Brayton cycle with hybrid solar/natural gas system,

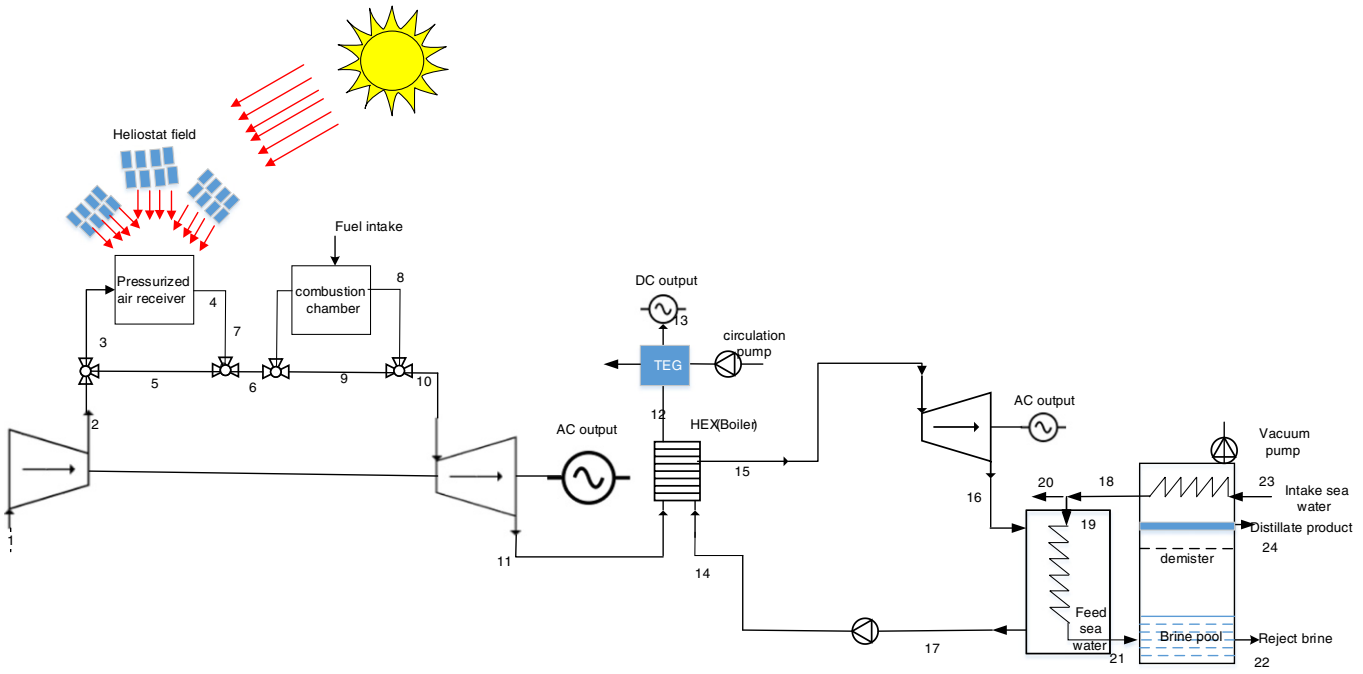

Fig. 1. Schematic of the present system.

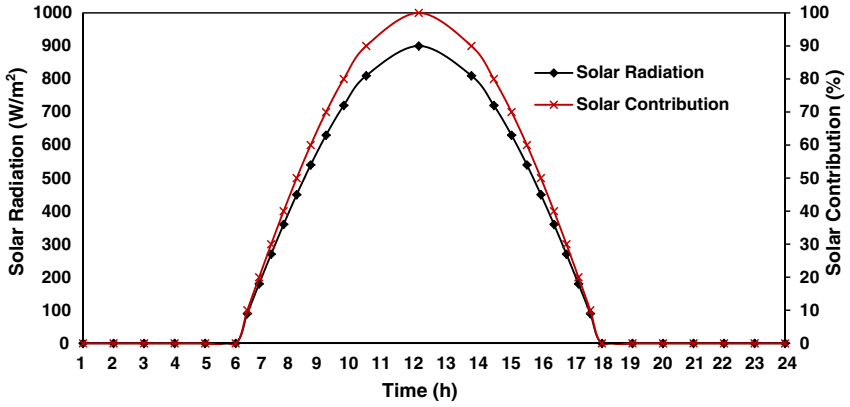

Fig. 2. Hourly variation of solar radiation and solar energy contribution to the Brayton Cycle.

Rankine cycle, integrated with flash distillation unit (FDU) and Thermoelectric generator unit (TEG) to generate electricity from waste heat.

In the proposed system, the compressor compresses air from 100 kPa to 1410 kPa. The compressed air flows to pressurized air receiver and heats up to 1207 K. When the solar radiation is not sufficient; natural gas compensates the deficient heat by burning in the combustion chamber. When solar radiation reaches its peak level, air stream by-passes the combustion chamber, and Brayton cycle runs with only solar power. On the other hand, after sunset, air stream by-passes solar receiver and directly flows to the combustion chamber. In Fig. 2, hourly variation of direct normal irradiance (DNI) and solar energy contribution to the Brayton Cycle can be seen. In this study, it is assumed that solar energy can be useful for 12 h per day, and maximum DNI is 900 W/m^2. The pressurized high-temperature air flows to the gas turbine to produce electricity. The exhaust gas of the Brayton cycle flows to heat exchanger (HEX 1) to generate steam for Rankine cycle. After the flue gas passes through the HEX 1, it enters the thermoelectric generator to produce electricity from waste heat.

Tin sulfide (SnS) and Bismuth Telluride (Be_2Te_3) are selected as thermoelectric materials for TEG. TEGs are installed on tubes and cover them all. While seawater is pumped by circulating pump flowing inside the tube, the hot flue gas flows around the tubes. Since a temperature difference occurs between both sides of TEG, electricity is generated. Geometry for TEG unit is modified version of parameterized shell-and-tube heat exchanger geometry in COMSOL [22]. Sketch of thermoelectric generator unit can be seen in Fig. 3.

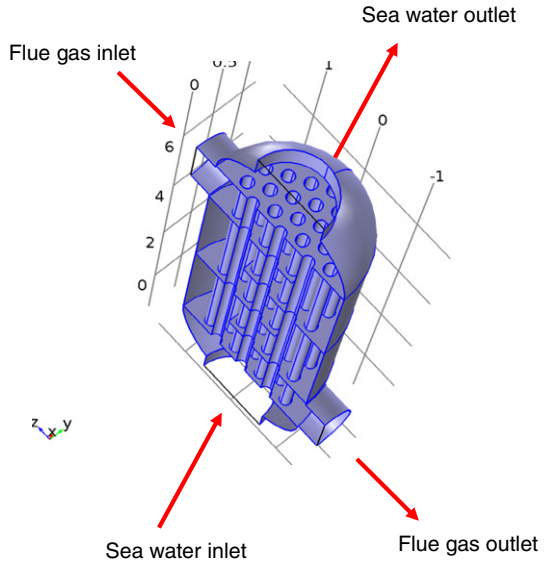

Fig. 3. TEG unit [22].

In parallel, the Rankine cycle also generates electricity. After the steam exits from steam turbine as wet steam, it enters a heat exchanger (HEX 2) to heat seawater up to 55 °C. Medium temperature seawater enters Flash Distillation Unit to produce distilled water at low pressure. At the beginning of the system, a vacuum pump runs for the set distillation tank pressure to reduce the pressure to 4.5 kPa.

3. Thermodynamic analyses

The energy and exergy efficiencies, exergy destructions, temperature, pressure, specific enthalpy and entropy are calculated for all system components. The combustion reaction is modelled on ASPEN Plus software package. TEG unit is modelled on COMSOL Multiphysics software package and rest of the components of the system is constructed in the Engineering Equation Solver (EES). The general design parameters and assumptions made for the analysis are listed in Table 1.

Beside parameters in Table 1, the following assumptions are made for the study:

- The changes in potential and kinetic energies are negligible.
- The only chemical reaction occurs in the combustion chamber.
- The heat losses to the environment occur only at heliostat surface.
- Ideal gas principles apply for the gases.

The energy balance, according to the first law of thermodynamics, is applied to each component of the system. Energy balance equation for

Table 1
Design parameters of the system.

Parameters	Value
Pressure ratio of compressor	14.1
Compressor isentropic efficiency	85%
Atmospheric conditions	100 kPa, 25 °C
Turbine isentropic efficiency	87%
Chamber combustion efficiency	95%
Electromechanical efficiency	95%
Air mass flow used	41.99 kg/s
Pressure of exhaust fumes	100 kPa
Direct normal irradiation (I)	900 W/m^2
Heliostat reflective area	11 × 11 m^2
Number of heliostats	300
Surface area of solar receiver area	60 m^2
Wind speed	5 m/s
Salinity of seawater	42,000 [ppm]

Table 2
Properties of thermoelectric materials used in TEG.

Properties (T = 400 K)	SnS [33]	Bi_2Te_3 [22]
k (W/m K)	0.05	1.75
σ(S/m)	379	59,400
S (V/K)	607e − 6	237e − 6

any component can be written as follows:

$$\dot{Q}-\dot{W}+\sum \dot{m}_{in}h_{in}-\sum \dot{m}_{out}h_{out}=0 \quad (1)$$

Here $\dot{Q}$ and $\dot{W}$ represent the heat transfer and work rate passing through the system boundaries, h represent the specific enthalpy of the working fluid and $\dot{m}$ represent the mass flow rate of working fluid.

Also, exergy balance is applied to each component of the system. Exergy balance equation for any component can be written as follows [23]:

$$\dot{Ex}^{Q_i}-\dot{Ex}_{W_i}+\sum \dot{m}_{in}ex_{in}-\sum \dot{m}_{out}ex_{out}-\dot{Ex}_{di}=0 \quad (2)$$

Here $\dot{Ex}^{Q_i}$ is the exergy transfer rate by heat, $\dot{Ex}_{W_i}$ represents exergy rate by work and $\dot{Ex}_{d_i}$ is exergy destruction rate by the component.

Specific exergies for each component also calculated for each component as follows:

$$ex_i=h_i-h_0-T_0(s_i-s_0)+ex_{ch} \quad (3)$$

Here ex_i is specific exergy for the i^{th} state point. h_0, T_0 and s_0 shows the specific enthalpy, temperature and specific entropy respectively for reference point which is ambient conditions T = 25 °C and P = 100 kPa. ex_{ch} represents the specific chemical exergy. The specific chemical exergy is calculated only for the state points where the chemical reaction occurs [24]. In this study, the only chemical reaction occurs in the combustion chamber. The calculation of specific chemical exergy can be written as follows [23]

$$ex_{ch}=\sum y_i\, ex_{ch,i}+R\,T_0\sum y_i \ln y_i \quad (4)$$

Here, y_i is the molar fraction of the gas species 'i' in the gas mixture. For instance, natural gas used in this study consists of 15% ethane and 85% methane, which makes y_i 0.15 and 0.85 for ethane and methane, respectively. $ex_{ch,i}$ represents standard chemical exergy of the gas species. Detailed exergy efficiency and exergy destruction rate definitions for each component are presented in Table 3.

Considering the main inputs and outputs of the system, the overall system energy and exergy efficiencies can be determined as follows:

$$\eta_{en,ov,sys}=1-\frac{\sum \dot{Q}_{out}}{\sum \dot{Q}_{in}} \quad (5)$$

$$\eta_{ex,ov,sys}=1-\frac{\sum Ex_d}{\sum Ex_{in}} \quad (6)$$

3.1. Energy inputs of the system

3.1.1. Pressurized solar receiver

The heat transfer rate between pressurized receiver and the stream can be calculated as follows:

$$\dot{Q}_r=\dot{Q}_h-\dot{Q}_{loss}=\dot{m}\,cp\,(T_4-T_3) \quad (7)$$

Here, $\dot{Q}_h$ is the thermal power received by the heliostat field and $\dot{Q}_{loss}$ is receiver loses by convection and radiation. $\dot{Q}_h$ can be calculated as follows [25]:

$$\dot{Q}_h=\eta_{field}\times I\times S_h\times N \quad (8)$$

Here, η_{field} is the solar effectiveness of heliostat field, I is direct normal irradiance (DNI), S_h is the reflective surface area of a heliostat and N is the number of heliostats.

$\dot{Q}_{loss}$ can be calculated as follows [25]

$$\dot{Q}_{loss}=h_aA_r(T_4-T_0)-\sigma_{SB}\,\varepsilon\left({T_4}^4-{T_0}^4\right) \quad (9)$$

Here h_a is heat transfer coefficient of air A_r is the surface area of the receiver, σ_{SB} is Stefan-Boltzmann constant and ε is Absorber emissivity. h_a is calculated by using following correlation [26]

$$h_a=10.45-v_a+10\sqrt{v_a}\ (W/(m^2K)) \quad (10)$$

Here v_a is wind speed in terms of (m/s).

3.1.2. Combustion chamber

In the combustion chamber, the natural gas is burned with the pressurized air when DNI is below 900 W/m^2. The heat input by combustion can be calculated as follow

$$\dot{Q}_c=\dot{m}_{fuel}\times LHV_{NG}\times\eta_c \quad (11)$$

Here, LHV_{NG} is lower heating value of natural gas and η_c is combustion efficiency. $\dot{m}_{fuel}$ is the mass flow rate of natural gas which varies

Table 3
Exergy efficiency and exergy destruction rate definitions for the system components.

Component	Exergy destruction rate definition	Exergy efficiency definition
Steam turbine	$\dot{Ex}_{d,ST}=\dot{m}_{15}ex_{15}-\dot{m}_{16}ex_{16}-\dot{W}_{out,ST}$	$\eta_{ex,ST}=\frac{\dot{W}_{out,ST}}{(\dot{m}_{15}ex_{15}-\dot{m}_{16}ex_{16})}$
Thermoelectric generator	$\dot{Ex}_{d,TEG}=\dot{m}_{12}ex_{12}-\dot{m}_{13}ex_{13}-\dot{W}_{out,TEG}$	$\eta_{ex,TEG}=\frac{\dot{W}_{out,TEG}}{(\dot{m}_{12}ex_{12}-\dot{m}_{13}ex_{13})}$
Pump	$\dot{Ex}_{d,P1}=\dot{m}_{17}ex_{17}+\dot{W}_{in,P}-\dot{m}_{14}ex_{14}$	$\eta_{ex,P}=1-\frac{\dot{Ex}_{d,P}}{\dot{Ex}_{in,P}}$
Heat exchanger 1	$\dot{Ex}_{d,HX1}=\dot{m}_{11}ex_{11}+\dot{m}_{14}ex_{14}-\dot{m}_{15}ex_{15}-\dot{m}_{12}ex_{12}$	$\eta_{ex,HX1}=\frac{(\dot{m}_{15}ex_{15}-\dot{m}_{14}ex_{14})}{(\dot{m}_{11}ex_{11}-\dot{m}_{12}ex_{12})}$
Heat exchanger 2	$\dot{Ex}_{d,HX2}=\dot{m}_{19}ex_{19}+\dot{m}_{16}ex_{16}-\dot{m}_{21}ex_{21}-\dot{m}_{17}ex_{17}$	$\eta_{ex,HX2}=\frac{(\dot{m}_{21}ex_{21}-\dot{m}_{19}ex_{19})}{(\dot{m}_{16}ex_{16}-\dot{m}_{17}ex_{17})}$
Gas turbine	$\dot{Ex}_{d,GT}=\dot{m}_{10}ex_{10}-\dot{m}_{11}ex_{11}-\dot{W}_{out,GT}$	$\eta_{ex,GT}=\frac{\dot{W}_{out,GT}}{(\dot{m}_{10}ex_{10}-\dot{m}_{11}ex_{11})}$
Compressor	$\dot{Ex}_{d,C}=\dot{m}_1ex_1+\dot{W}_{in,C}-\dot{m}_2ex_2$	$\eta_{ex,C4}=\frac{(\dot{m}_2ex_2-\dot{m}_1ex_1)}{\dot{W}_{in,C}}$
Solar receiver	$\dot{Ex}_{d,SR}=\dot{m}_3ex_3-\dot{m}_4ex_4+\dot{Q}_{SR}(1-\frac{T_0}{T_{sun}})$	$\eta_{ex,SR}=\frac{(\dot{m}_3ex_3-\dot{m}_4ex_4)}{\dot{Q}_{SR}(1-\frac{T_0}{T_{sun}})}$

Table 4
Mesh statistics.

Description	Value
Tetrahedral elements	105,180
Pyramid elements	10,240
Prism elements	72,785
Triangular elements	20,653
Quadrilateral elements	1613
Edge elements	3892
Vertex elements	432
Total elements	214,795

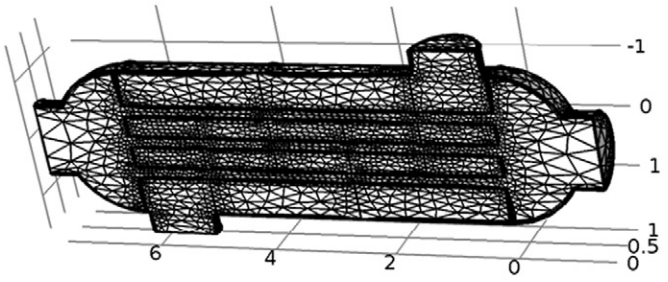

Fig. 4. Meshes of TEG unit [22].

with changing DNI. In this study, LHV is taken 47,141 MJ for the natural gas [27].

3.2. Thermoelectric generator

The thermoelectric effect is considered a phenomenon that provides direct and reversible conversion between thermal and electrical energy. This phenomenon is also known as "Seebeck Effect" where a thermoelectric generator is utilized to produce electricity from temperature difference and "Thompson Effect" where a thermoelectric generator is utilized to produce cooling effect through a voltage difference.

A dimensionless figure of merit is defined to demonstrate the thermoelectric performance. Thermal efficiency of a TEG is related to $Z\overline{T}$. As the value of $Z\overline{T}$increases, thermodynamic performance of the TEG increases as well. $Z\overline{T}$ can be calculated as

$$Z\overline{T} = \frac{(S_p - S_n)^2 \overline{T}}{\left[\left(\frac{k_n}{\sigma_n}\right)^{\frac{1}{2}} + \left(\frac{k_p}{\sigma_p}\right)^{\frac{1}{2}}\right]^2} \tag{12}$$

Here, k σ and S represent thermal conductivity (W/m K), electrical conductivity (S/m) and Seebeck coefficient (V/K) respectively. Every thermoelectric device consists of two type of thermoelectric material as p and n-type. Those semiconductor materials are connected from their ends. p and n indices refer to legs of the thermoelectric generator. A good thermoelectric material should have large thermal resistance to increase temperature difference between hot and cold side of it. Maximizing S and σ are also increase the value of $Z\overline{T}$

The thermal efficiency of TEG is defined as [28]:

$$\eta_{TEG} = \frac{\dot{W}_{TEG}}{\dot{Q}_{TEG}} = \frac{T_H - T_C}{T_H} \frac{\sqrt{1 + Z\overline{T}} - 1}{\sqrt{1 + Z\overline{T}} - \frac{T_C}{T_H}} \tag{13}$$

where $\overline{T}$is the average temperature between the hot (T_H) and cold sides (T_C) of thermoelectric material.

Here, $\dot{W}_{TEG}$is generated power by TEG and $\dot{Q}_{TEG}$ is the heat transfer rate between cold and hot side of TEG. Tin sulfide (SnS) and Bismuth Telluride (Be_2Te_3) are selected as thermoelectric materials for TEG where the properties of selected thermoelectric materials are presented in Table 2.

In order to determine $\dot{Q}_{TEG}$,T_H and T_c, a numerical analysis is done by COMSOL Multiphysics Software Package. k-ε turbulence model is used in the numerical analysis to model turbulent flow in TEG. The numerical study is conducted under steady state conditions. Mesh elements used in the numerical study can be seen in Fig. 3 whereas the mesh statistics are presented in Table 4. (See Fig. 4.)

Seven different mesh elements are used in the current numerical study. They are distributed in the model according to physic of the problem. Mesh frequency is increased closer to the wall. When the DNI is 450 W/m^2, hot side of TEG is fed by 500 °C flue gas temperature with 42.26 kg/s mass flow rate and cold side of TEG is fed by seawater pumped by circulating pump with temperature 20 °C and speed 5 m/s. Under these conditions, $\dot{Q}_{TEG}$ is determined as 1627.5 kW and

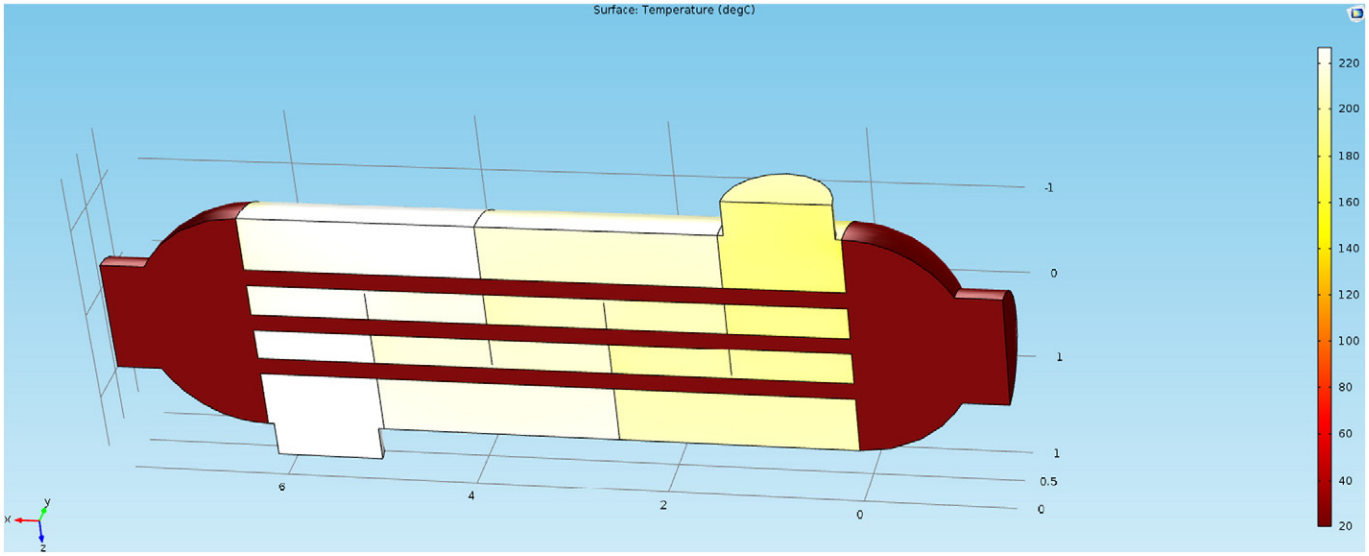

Fig. 5. Temperature distribution of TEG unit [22].

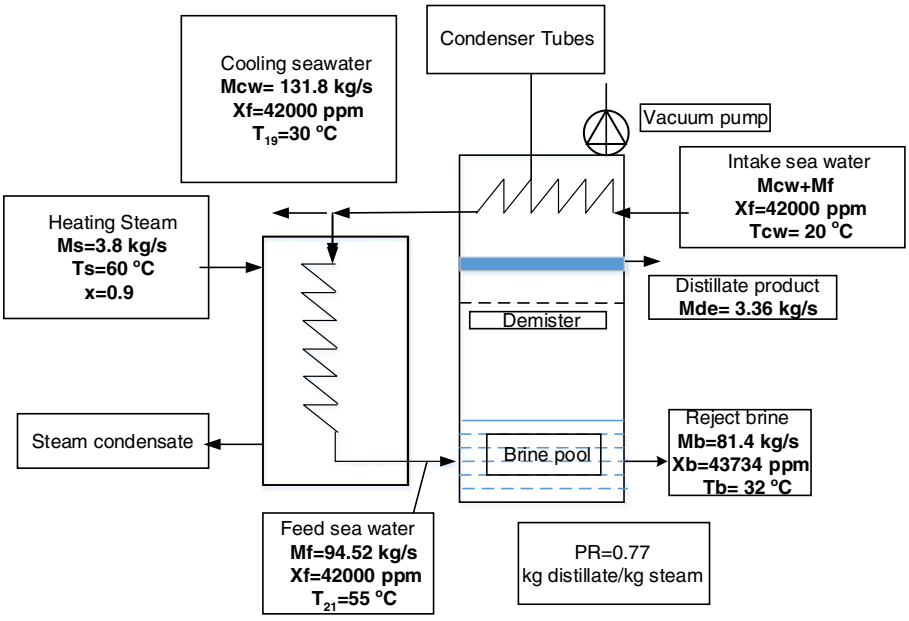

Fig. 6. Flash distillation unit.

thermal efficiency of TEG η_{TEG} is determined as 2.02%. It means 32.94 kW electricity can be produced by TEG. It is important for a thermoelectric generator to keep temperature difference between cold and hot sides as much as possible, because efficiency is highly dependent on the temperature difference. The temperature distribution on TEG unit can be seen in Fig. 5. As it is presented in Fig. 5, the temperature of water inlet and exit of TEG unit slightly changes. It can be attributed to two main reasons: Firstly, thermal conductivity of TEG has small value (1.5 W/m K), secondly water passes through the TEG unit in 1.2 s.

3.3. Flash distillation unit

A single-stage flash distillation unit (FDU) used in the system is shown in Fig. 6. The seawater comes to the system with 20 °C and heated up by the wet steam, which leaves the steam turbine. The temperature of the seawater reaches 55 °C when it leaves the heat exchanger. After seawater heats up, it enters the FDU and condensates at low-pressure media and distillate product is collected for domestic purposes. The system designed as an open system. Heat rejection of the system is provided by seawater pumped by a circulation pump. Brine water is rejected to sea at about 32 °C.

Multiple effect distillation plants and multiple stage flash distillation plants are considered thermodynamically more efficient than single stage distillation units. The number of their stages can reach more than 20 stages which increase the required space for these units. Moreover, most of MSF plants operate at top brine temperatures of 90–120 °C [29]. The brine temperature decreases gradually in every stage. In this study, top brine temperature is only 55 °C, which is relatively low for multiple stage distillation processes. [29]. On the other hand, the single stage distillation units are considered to be an excellent option for seawater distillation when the compact size of the design is important. Furthermore, such systems are treated as a feasible option where there is surplus and inexpensive heat.

In this study, the heat extracted from the condenser of the Rankine cycle is aimed to be used for distillation purposes. A single flash distillation system is selected based on the following criteria: low steam temperature, low cost, smaller and more compact design, smaller capacities, etc. In Table 5 [30], some of small scaled desalination plants are listed. The desalination capacity of listed plants varies from 125 m^3/day to 586 m^3/day. In this study, the desired capacity of desalination plant is targeted to be at least 250 m^3/day. The desalination model is built on the following assumptions [31]:

- The distillate product is salt-free.
- The specific heat of seawater is taken as 4.18 kJ/kg K.
- The subcooling of condensate and superheating of heating steam have a negligible effect on the system energy balance.
- The power requirements for vacuum pump are not included in the system analysis.
- The heat losses from the system are negligible.

The total mass balance of the system can be written as [31]:

$$\dot{m}_f = \dot{m}_b + \dot{m}_{de} \quad (14)$$

Table 5
Examples of small scaled desalination plants [30].

Location	Desalination capacity (m^3/day)	Application
Belawan, Indonesia	500	Drinkable water supply
Das Islands, Abu Dhabi	125	Drinkable water supply in the island
Al-Murrawah, Abu Dhabi	500	Drinkable water
Skikda, Algeria	380	Drinkable water
Farazan Islands, Saudi Arabia	140	Drinkable water supply in the island
Royal Haymen Resort, Australia	270	Drinkable water supply to holiday resort
St. John, US Virgin Islands	586	Drinkable water supply in the island
Las Banos, California USA	190	VC concentrator
Municipality of Uwa Jima, Japan	180	Municipal water supply

Table 6
Measured and calculated values of Nafey's study.
Source: [26].

Exp. #	Time	T_{fi}(°C)	T_{fo}(°C)	TBT(°C)	T_b(°C)	T_d (°C)	$M_{d,exp.}$ (kg/h)	$M_{d,theo}$ (kg/h)
1	11	27	38	54	41	39	1.40	1.67
2	12	27	39	56	42	40	1.66	1.79
3	13	27	37	52	40	38	1.56	1.74
4	14	27	36	50	39	37	1.26	1.47

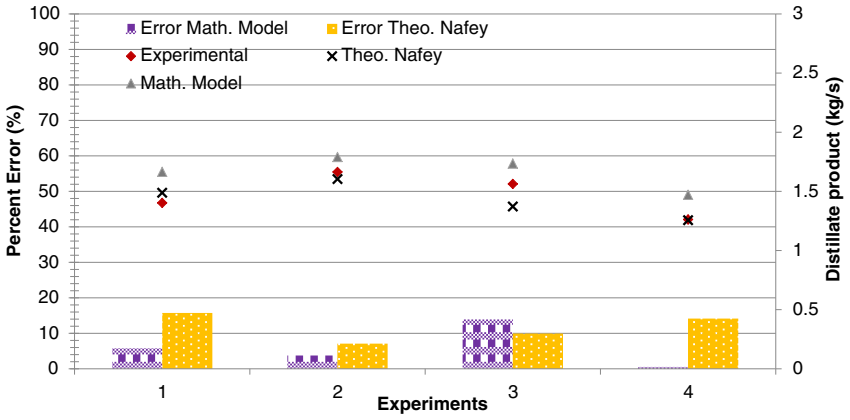

Fig. 7. Measured and calculated distillate product by the FDU.

$$X_f \dot{m}_f = X_b \dot{m}_b \tag{15}$$

Here $\dot{m}_f$, $\dot{m}_b$, and $\dot{m}_{de}$, are mass flow rate of feed seawater, brine water and distillate product respectively. X_f and X_b represent salinity of feed seawater and brine water.

The brine heater and condenser energy balances can be written as [31]:

$$\dot{m}_{16}\, h_{fg,water} = \dot{m}_f\, Cp\,(T_{19} - T_{21}) \tag{16}$$

$$\dot{m}_{de}\, h_{fg,vapor} = (\dot{m}_{cw} + \dot{m}_f)\, Cp\,(T_{21} - T_{cw}) = \dot{m}_f\, Cp(T_{21} - T_b) \tag{17}$$

where T_b and T_{cw} are brine and intake seawater temperature respectively.

The heat transfer rate between wet steam from turbine and seawater can be written as:

$$\dot{m}_{16}\, h_{fg,water} = U_h\, A_h\, (LMTD)_h \tag{18}$$

$$(LMTD)_h = (T_{21} - T_{19}) / \ln\left((T_{16} - T_{19})/(T_{16} - T_{21})\right) \tag{19}$$

where U_h is overall heat transfer coefficient at brine heater and A_h is heat transfer area of it. $(LMTD)_h$ is the logarithmic mean temperature difference at brine heater. Similarly heat transfer rate for the condenser can be written as

$$\dot{m}_{de}\, h_{fg,vapor} = U_c\, A_c\, (LMTD)_c \tag{20}$$

$$(LMTD)_c = (T_{19} - T_{cw}) / \ln\left((T_v - T_{cw})/(T_v - T_{19})\right) \tag{21}$$

The PR of the system represents the amount of distilled product per used steam. It can be determined by dividing Eq. (16) and Eq. (17) [31]:

$$PR = \frac{\dot{m}_{de}}{\dot{m}_{16}} = \frac{\dot{m}_f\, Cp\,(T_{21} - T_b) h_{fg,vapor}}{\dot{m}_f\, Cp\,(T_{19} - T_{21}) h_{fg,water}} \tag{22}$$

The desalination model is built with the help of a reference book [31] with specific details of the model provided in the sixth chapter. The experimental and theoretical studies of Nafey et al. [20] are used for validation of the model. They built a small flash desalination unit for water by solar energy and made a both theoretical and experimental study. Their experimental setup is quite similar to the FDU used in this study. Their system consists of a brine heater and a vertical flash unit. The flash unit is connected to a condenser/preheater. Measured results and theoretical findings calculated by

Table 7
Thermodynamic data for all state points when the solar contribution is 50%.

State no.	Stream	T (K)	P (kPa)	$\dot{m}$ (kg/s)	h (kJ/kg)	s (kJ/kg K)	ex (kJ/kg)
0	Air	298.2	100	–	104.8	0.3669	–
0`	Water	298.2	100	–	298.4	6.864	–
1	Air	298.2	100	41.99	298.4	6.864	0
2	Air	706.3	1410	41.99	720.8	6.991	384.50
3	Air	706.3	1400	41.99	720.8	6.993	383.90
4	Air	940.8	1400	41.99	980.2	7.31	548.87
6	Air	940.8	1393	41.99	980.2	7.311	548.42
7	Air	940.8	1386	41.99	980.2	7.313	547.99
8	Combustion gases	1187	1386	42.26	1264	7.58	751.82
10	Combustion gases	1187	1376	42.26	1264	7.582	751.21
11	Combustion gases	743	100	42.26	760.3	7.807	180.83
12	Combustion gases	500	100	42.26	503.5	7.389	48.60
13	Combustion gases	462.5	100	42.26	464.9	7.309	33.96
14	Water	334.2	800	3.717	256	0.8433	9.12
15	Water	630	800	3.717	3176	7.431	964.76
16	Water	333.2	19.93	3.717	2373	7.431	161.90
17	Water	333.2	19.93	3.717	251.2	0.8312	7.89
18	Water	303.2	100	127.5	125.8	0.4365	0.17
19	Seawater	303.2	100	81.98	125.8	0.4365	0.17
20	Seawater	303.2	100	45.55	125.8	0.4365	0.17
21	Seawater	328.2	100	81.98	230.3	0.7679	5.92
22	Brine water	305.2	4.495	78.73	129.9	0.4503	0.15
23	Seawater	293.2	100	127.5	83.93	0.2962	0.18
24	Distillate product	304.2	4.495	3.25	129.9	0.4503	0.15

Table 8
Thermodynamic analysis results of the developed system when the solar contribution is 50%.

Component	Exergy destruction rate (kW)	Exergy efficiency (%)	Work rate or heat transfer rate (kW)
Compressor	1587	91.05	17,733
Valve 1	25.04		
Solar receiver	3404	59.62	10,893
Valve 2	18.77		
Valve 3	18.77		
Combustion chamber	5984		12,251
Valve 4	25.91		
Gas turbine	4954	79.45	19,150
TEG	585.8	5.32	32.94
Pump	13.43	54.23	17.98
HEX 1	2036	63.57	
Steam turbine	352.1	88.2	2632
HEX 2	101.6	82.26	
Flash distillation unit	473.1		

them are presented in Table 6. In Table 6, T_{fi}, T_{fo}, TBT, T_b, T_d, $M_{d,exp.}$ and $M_{d,theo}$ represent; Inlet feed temperature of the condenser, Outlet feed temperature of the condenser, The top brine temperature, outlet brine stream temperature from the flash stage, distillate product stream temperature, experimental distillate product rate and Theoretical distillate product rate respectively. The measured conditions are applied to the mathematical model used in this study and compared with Nafey's study. Comparison of distillate products can be seen in Fig. 7.

In Fig. 7, the Percent error is calculated by following equation:

$$Error = \frac{|Measured - Calculated|}{Calculated} \times 100 \quad (23)$$

The average percent error for the mathematical model used in this study is obtained 6%, which is within the permissible range.

4. Results and discussion

Thermodynamic calculations of each system components are performed by using Engineering Equation Solver (EES) software. The values of temperature (K), pressure (kPa), mass flow rate (kg/s), specific enthalpy (kJ/kg), specific entropy (kJ/kg K), and specific exergy (kJ/kg) are determined for the each state point of the system as listed in Table 7.

The values of exergy destruction rate (kW), exergy efficiency (%), work rate or heat transfer rate (kW) of each system component are presented in Table 8. Tables 7 and 8 present the values when the solar contribution to the system is 50% (DNI = 450 W/m^2).

As seen in Table 8 and Fig. 8, the maximum exergy destruction rates are determined in combustion chamber and gas turbine. It is because of high irreversibility of the components. The exergy efficiency of the gas turbine is observed as almost 80%. As presented in Table 8 and Fig. 8, the exergy destruction rates of valves and pump have the lowest share in the overall system. The heat losses at solar receiver are taken into account in this study. Hence, it causes large exergy destruction rate on this component. Another reason of this situation can also be explained as the heat transfer through solar receiver occurs at high-temperature differences. To decrease the exergy destruction rate on this component, the heat losses need to be decreased. Fig. 9 presents exergy efficiencies of

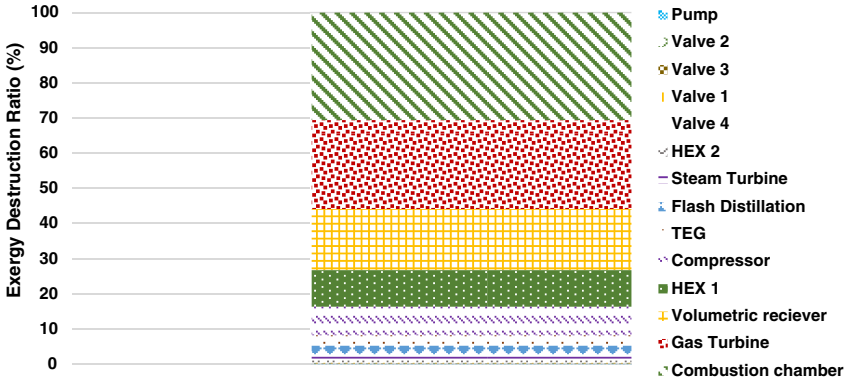

Fig. 8. Exergy destruction ratios in the system.

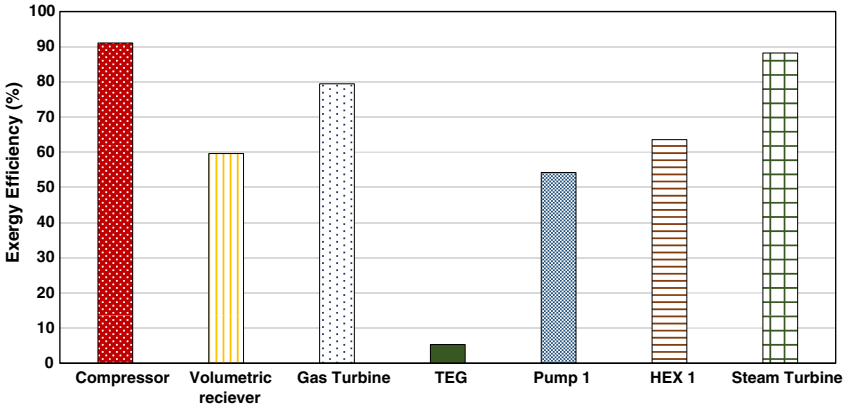

Fig. 9. Exergy efficiencies of system components when the solar contribution is 50%.

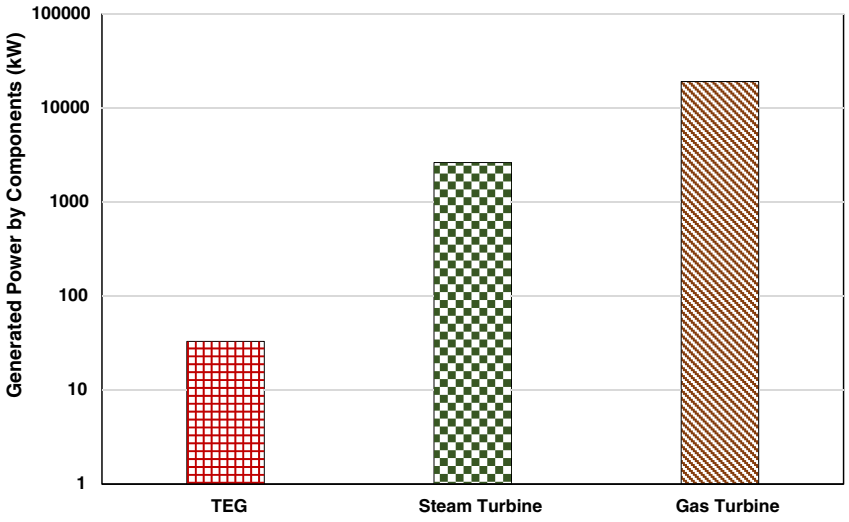

Fig. 10. Generated power by system components.

each component of the system when DNI is 450 W/m^2. The compressor has the highest exergy efficiency with 91% and thermoelectric generator has smallest exergy efficiency with 5.32%. The main reason of low exergy efficiency of thermoelectric generator is thermoelectric generators` power generation capacity. Since the energy efficiency of TEG is 2%, it causes low energy production relatively to heat transfer rate between the hot and cold side of TEG.

The generated power by system components are comparatively presented in Fig. 10. As it is expected, the lowest power is produced by TEG and highest power is generated by the gas turbine. 19,150 kW, 2632 kW and 32.94 kW electricity produced by the gas turbine, steam turbine and TEG respectively. The flash distillation unit produces 290 m^3 fresh water per day. The FDU capacity is in the same range as the desalination plants in Table 5.

4.1. Parametric studies

4.1.1. Effects of direct normal irradiance

Fig. 11 represents the change of the overall energy and exergy efficiencies throughout a day. As it can be seen in Fig. 11, the exergy efficiency is more depended on solar contribution. The reason of that, as it shown in Fig. 8, the exergy destruction rate of combustion chamber has larger values relatively. As the mass flow rate of natural gas decreases, the exergy destruction rate of combustion chamber decreases, too resulting in higher exergy efficiencies.

In Fig. 12, the mass flow rate of CO_2 emission and mass flow rate of natural gas are presented at each hour in a day. As the mass flow rate of fuel increases, the CO_2 emission level also increases. It reaches maximum level (1.5 kg/s) when the solar contribution is 0%. When the direct normal irradiance reaches 900 W/m^2, the carbon emission level lowers down to 0 kg/s.

4.1.2. Effects of temperature of seawater

Fig. 13 presents the change of performance ratio and seawater intake of the flash distillation unit with seawater temperature. According to Fig. 13, as the sea temperature increases, there is less intake seawater requirement to produce the same amount of fresh water. As the seawater temperature increases, the required heat transfer rate will be less to reach the same top brine temperature. Therefore, the flow rate of water intake water will be smaller. However, the performance ratio of FDU also decreases with seawater temperature.

4.1.3. Effects of TEG cooling side heat rejection type

In this section, heat rejection from the cool junction of the thermoelectric generator is investigated. In order to produce electricity from the thermoelectric material, the temperature difference between hot and cold sides should be maintained. In the proposed design, hot and cold sides of the thermoelectric material are provided by flue gas and seawater pumped by circulating pump respectively. To see the effect of heat rejection type from TEG, two

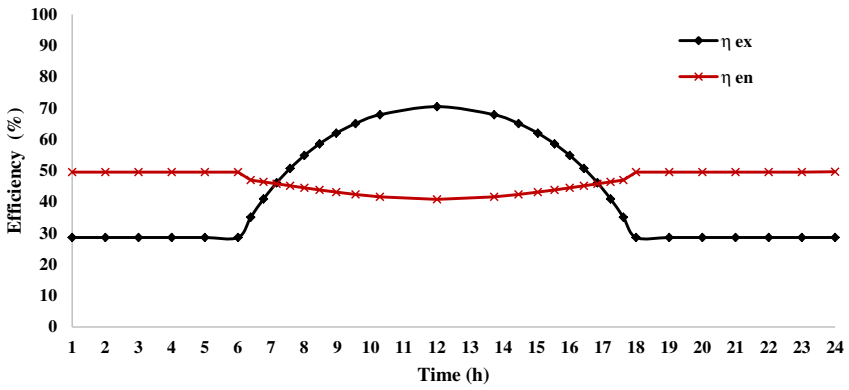

Fig. 11. Hourly variation of Energy and Exergy Efficiencies.

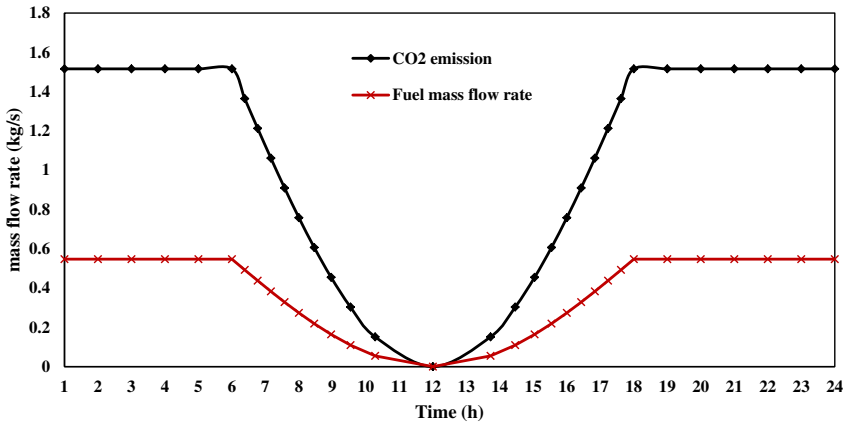

Fig. 12. Hourly variation of CO_2 and fuel mass flow rate.

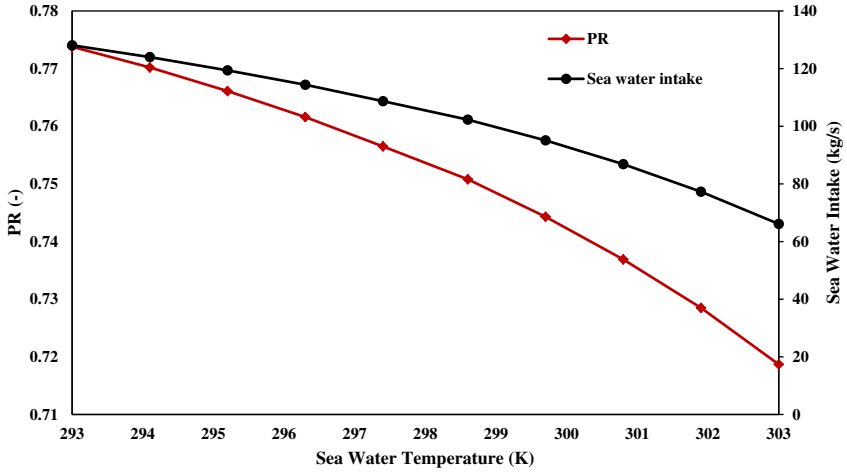

Fig. 13. Performance Ratio and Water intake of the FDU variation with Seawater Temperature.

more alternative cool side cooling are proposed. First one is cooling with the ambient wind without any component and the second one is cooling with the help of a blower which blows the air instead of pumping the seawater. Air velocity after blower is 15 m/s.

In Fig. 14, Power generation by TEG with three cool side options is presented. It can be seen in the figure that the highest power can be generated from circulating pump option and the least power is generated by natural cooling option. The main reason for this situation

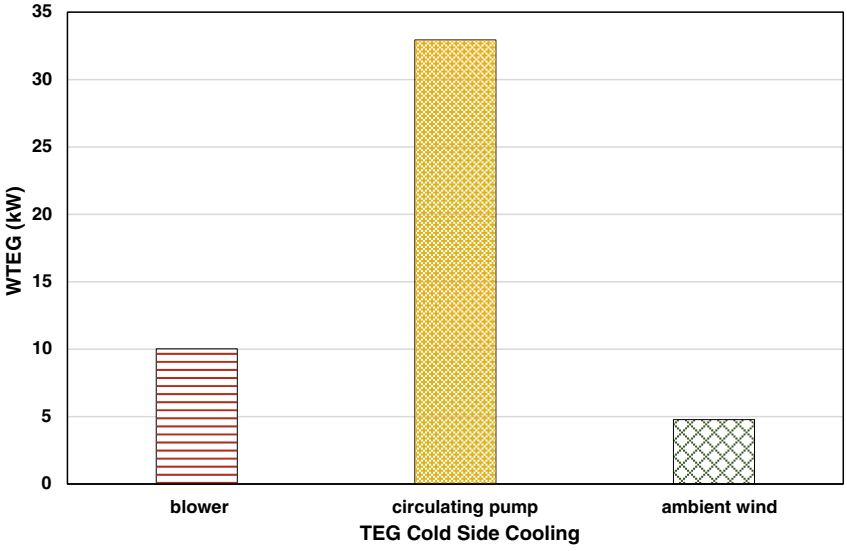

Fig. 14. Power generated by TEG with different cool side cooling.

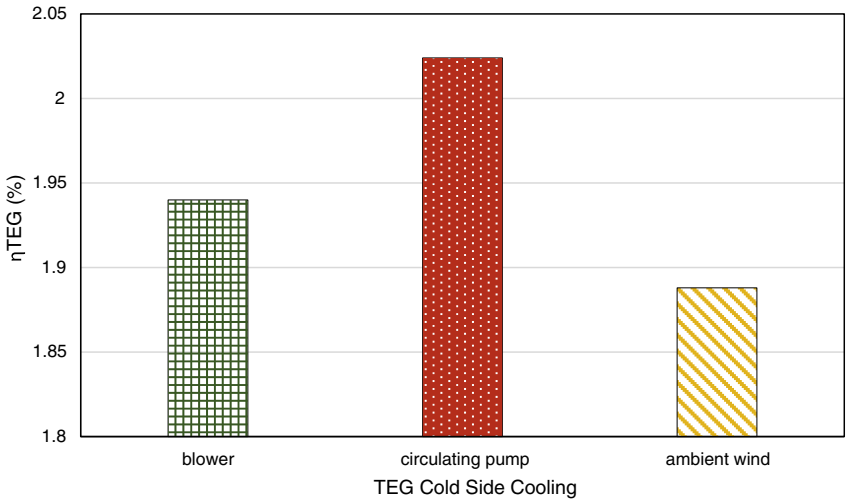

Fig. 15. Power generated by TEG with different cool side cooling.

is, the highest heat transfer rate between hot and cold side occurs for the option with circulating pump. Because the convective the heat transfer coefficient for that option is highest (Nu (Re, Pr)). Second reason is also the highest efficiency of TEG observed for circulating pump option. These efficiencies are illustrated in Fig. 15. As a result of the highest efficiency and heat transfer rate, cooling with the circulating pump option has the highest produced power. Even though, circulation pump requires 2.5 kW, option with the pump still has the highest net power production. In Fig. 15, it can also be observed that cooling with ambient wind option has the lowest efficiency. Its main reason is cooling with ambient air is not efficient. Cp of air is less than Cp of water when they are compared. Specific heat differences cause a substantial temperature rise in cold side of TEG. The efficiency of TEG highly depends on the temperature difference between hot and cold sides. As the lowest temperature difference is observed in the ambient cooling, it has the lowest efficiency.

5. Conclusions

In this study, a water-electric cogeneration system integrated with a thermoelectric generator is investigated and analyzed. The thermodynamic quantities, energy and energy efficiencies for each component are calculated. The performance of the overall system during the day hours is determined. The following concluding remarks can be stated:

- The overall exergy efficiency is obtained as 54.9% at 50% solar contribution.
- The overall energy efficiency is obtained as 44.5% at 50% solar õcontribution.
- As the maximum exergy destruction rates are determined in combustion chamber and gas turbine, the overall exergy efficiency increases with solar contribution.
- The system has 21.8 MW of generating electricity capacity.
- By installation of a circulating pump to TEG unit, it is possible to increase the generated power more than 28 kW.
- The heat-to-electricity conversion efficiency of the TEG is found to be 2.02%.
- It produces 3.36 kg/s of fresh water.
- The amount of produced fresh water can be increased by increasing wet steam temperature which leaves the Rankine cycle.
- Desalination unit produces 280,775 kg fresh water per day. It can provide fresh water demand for a community having slightly more than 1000 people. The proposed system is feasible for small towns. For larger communities, overall system should be scaled up. Additional flashing stages can be added to the system to convert it to an MSF unit.

References

[1] EuropeanComission, SOLGATE Solar Hybrid Gas Turbine Electric Power System(Final Publishable Report. Energy) , 2005, ISBN 92-894-4592-0.
[2] S. Peng, H. Hong, H. Jin, Z. Wang, An integrated solar thermal power system using intercooled gas turbine and Kalina cycle, Energy 44 (2012) 732–740.
[3] I.E. Meriche, A. Baghidja, T.E. Boukelia, Design and Performance Evaluation of Solar Gas Turbine Power Plant in South Western Algeria, 2014 4.
[4] X.F. Zheng, C.X. Liu, R. Boukhanouf, Y.Y. Yan, W.Z. Li, Experimental study of a domestic thermoelectric cogeneration system, Appl. Therm. Eng. 62 (2014) 69–79.
[5] B. Orr, B. Singh, L. Tan, A. Akbarzadeh, Electricity generation from an exhaust heat recovery system utilising thermoelectric cells and heat pipes, Appl. Therm. Eng. 73 (2014) 588–597.
[6] S.A. Omer, D.G. Infield, Design and thermal analysis of a two stage solar concentrator for combined heat and thermoelectric power generation, Energy Convers. Manag. 41 (2000) 737–756.
[7] A.Z. Sahin, B.S. Yilbas, S.Z. Shuja, O. Momin, Investigation into topping cycle: thermal efficiency with and without presence of thermoelectric generator, Energy 36 (2011) 4048–4054.
[8] O. Francis, O. IK, A. AM, Improved Efficiency Performance of a Gas Turbine with a Thermoelectric Generator, vol. 3, 2012 1–8.
[9] A. Ghobeity, A. Mitsos, Optimal design and operation of desalination systems: new challenges and recent advances, Curr. Opin. Chem. Eng. 6 (2014) 61–68.
[10] F. Khalid, I. Dincer, M.A. Rosen, Comparative assessment of CANDU 6 and sodium-cooled fast reactors for nuclear desalination, Desalination 379 (2016) 182–192.
[11] E. Cardona, S. Culotta, A. Piacentino, Energy saving with MSF-RO series desalination plants, Desalination 153 (2003) 167–171.
[12] M.N.A. Hawlader, P.K. Dey, S. Diab, C.Y. Chung, Solar assisted heat pump desalination system, Desalination 168 (2004) 49–54.
[13] R. Deng, L. Xie, H. Lin, J. Liu, W. Han, Integration of thermal energy and seawater desalination, Energy 35 (2010) 4368–4374.
[14] B. Ortega-Delgado, L. Garcia-Rodriguez, D.C. Alarcon-Padilla, Thermoeconomic comparison of integrating seawater desalination processes in a concentrating solar power plant of 5 MWe, Desalination 392 (2016) 102–117.
[15] P. Palenzuela, D.C. Alarcón-Padilla, G. Zaragoza, Large-scale solar desalination by combination with CSP: techno-economic analysis of different options for the Mediterranean Sea and the Arabian gulf, Desalination 366 (2015) 130–138.
[16] P. Palenzuela, G. Zaragoza, D. Alarcón, J. Blanco, Simulation and evaluation of the coupling of desalination units to parabolic-trough solar power plants in the Mediterranean region, Desalination 281 (2011) 379–387.
[17] P. Palenzuela, G. Zaragoza, D.C. Alarcón-padilla, E. Guillén, M. Ibarra, Assessment of different con fi gurations for combined parabolic-trough (PT) solar power and desalination plants in arid regions, Energy 36 (2011) 4950–4958.
[18] G. Iaquaniello, A. Salladini, A. Mari, A.A. Mabrouk, H.E.S. Fath, Concentrating solar power (CSP) system integrated with MED – RO hybrid desalination, Desalination 336 (2014) 121–128.
[19] O. Ahmed, H. Kosaka, K.H. Bamardouf, K. Al-shail, A.S. Al-ghamdi, Concentrating solar power for seawater thermal desalination, Desalination 396 (2016) 70–78.
[20] A.S. Nafey, M.A. Mohamad, S.O. El-Helaby, M.A. Sharaf, Theoretical and experimental study of a small unit for solar desalination using flashing process, Energy Convers. Manag. 48 (2007) 528–538.

[21] L. García-Rodríguez, C. Gómez-Camacho, Conditions for economical benefits of the use of solar energy in multi-stage flash distillation, Desalination 125 (1999) 133–138.
[22] COMSOL, Multiphysics® Modeling Software Version 5.2Available from https://www.comsol.com/.
[23] I. Dincer, M.A. Rosen, Chapter 2 - exergy and energy analyses, Exergy, Elsevier, Amsterdam 2013, pp. 21–30, http://dx.doi.org/10.1016/B978-0-08-097089-9.00002-4.
[24] Y. Bicer, I. Dincer, Energy and exergy analyses of an integrated underground coal gasification with SOFC fuel cell system for multigeneration including hydrogen production, Int. J. Hydrog. Energy 40 (2015) 13323–13337.
[25] I.E. Meriche, A. Beghidja, M. Boumedjirek, Energetic and exergetic analysis of solar gas turbine power plant in South AlgerialREC 2014 - 5th International Renewable Energy Congress, 2014, http://dx.doi.org/10.1109/IREC.2014.6826902.
[26] European Regional Development Fund, European Neighbourhood and Partnership Instrument, Radiant heating, convection heating systems and wall tempering, WP5 Educ. Econ. Promot 2014, p. 1 (CO2OL Bricks).
[27] B. Boundy, S. Diegel, L. Wright, S.C. Davis, Biomass Energy Data Book, 4 ed.4, 2011 254.
[28] X. Zhang, L.-D. Zhao, Thermoelectric materials: energy conversion between heat and electricity, J. Mater. 1 (2015) 92–105.
[29] R. Saidur, E.T. Elcevvadi, S. Mekhilef, A. Safari, H.A. Mohammed, An overview of different distillation methods for small scale applications, Renew. Sust. Energ. Rev. 15 (2011) 4756–4764.
[30] H.K. Sadhukhan, P.K. Tewari, Small Desalination Plants (SDPS), Desalination and Water Resources, Thermal desalination processes, vol. II, 2010, pp. 346–356.
[31] H.T. El-Dessouky, H.M. Ettouney, Fundamentals of Salt Water Desalination, Elsevier, 2002, http://dx.doi.org/10.1016/B978-044450810-2/50008-7.
[33] G. Ding, G. Gao, K. Yao, High-efficient thermoelectric materials: the case of orthorhombic IV-VI compounds, Sci. Rep. 5 (2015) 9567.